Renewable Energy 239 (2025) 121974

Contents lists available at ScienceDirect

Renewable Energy

journal homepage: www.elsevier.com/locate/renene

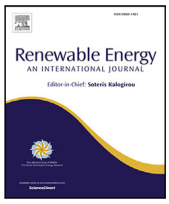

Fast optimal control performance evaluation for wave energy control co-design

Zechuan Lin [a,b], Xuanrui Huang [a], Xi Xiao [a,*], John V. Ringwood [b]

[a] Department of Electrical Engineering, Tsinghua University, Beijing 100084, China
[b] Centre for Ocean Energy Research, Maynooth University, Co. Kildare, Ireland

ARTICLE INFO

Keywords:
Wave energy converter
Control co-design
Model predictive control
Pseudo-spectral control

ABSTRACT

With the application of energy-maximizing control for wave energy converters (WECs), the WEC design problem becomes a control co-design problem. One of the fundamental requirements of co-design is to evaluate the optimal control performance, i.e., average power generation. Previous control techniques include model predictive control (MPC) and pseudo-spectral (PS) control, but both require iterative optimization, with computational requirements the main limiting factor in co-design. In this study, a fast optimal control performance evaluation method is proposed based on a 'wave-by-wave' (WbW) representation. The idea is to split the wave excitation force (WEF) signals into individual waves, process them separately, and then combine the results with the distribution of WEF amplitude and period, yielding a straightforward average power calculation. The method is fully developed and studied, considering the cases of position-only, and general, constraints, as well as different choices to obtain the WEF parameter distribution. It is shown that the WbW method can achieve a very high control evaluation fidelity (within a 5% error) and give almost the same co-design result as MPC and PS (implemented using WecOptTool), but with a significantly reduced computation time (e.g., hundreds of times faster), therefore being a game changer for control co-design of WECs.

1. Introduction

Rapidly developed in the last decade, advanced control for wave energy converters (WECs) is recognized to be one of the most effective techniques to improve their power capture efficiency and lower the levelized cost of energy (LCoE) [1]. Compared with traditional WEC controllers that work passively, advanced controllers such as the reactive control [2], latching control [3], and constrained model predictive control (MPC) [4] can actively manipulate the WEC dynamics so that more energy can be captured by the device.

However, with advanced control involved, the WEC design problem, i.e., to determine the best geometry, mechanical and power take-off (PTO) limits, or other design parameters, becomes more complex, due to the contribution of the WEC *and* controller parameters to the overall WEC dynamics. Consequently, the 'optimal' WEC design parameters are highly dependent on the controller [5]. Hence, the original design process becomes a *control co-design* process, which is widely adopted for wind power systems [6].

Ideally, one would want to use the optimal controller to maximize power capture within device constraints, and accordingly, one needs to design the WEC based on this optimal controller. In fact, MPC is recognized to represent the optimal constrained performance [7] and has seen successful implementations [8]. MPC typically works by solving receding-horizon control problems with time-domain discretization. If such a controller is to be used for co-design, in order to evaluate the performance, e.g., the annual average power for any given set of design parameters: (i) Time-domain simulation of the WEC system is needed, (ii) In each simulation, a series of receding-horizon optimization problems need to be solved, and (iii) the simulation should be repeated for multiple sea states in a given sea area, and for multiple phase realizations for each sea state [9]. As a result, the co-design process can be computationally prohibitive. Hence, it is of great value to find a control performance evaluation method that gives the same performance as MPC but is more computationally efficient. Since control co-design is an off-line calculation, i.e., it is not necessary to simulate a real-time controller that only uses currently available information, a 'global' representation of the system suffices to *evaluate* the performance. However, while it is possible to adopt a 'global' MPC, with a control horizon covering the entire operating (evaluation, in a co-design setting) time of the device, the corresponding optimization problem may face too a large dimension. Alternatively, the global

* Corresponding author.
E-mail addresses: xiao_xi@tsinghua.edu.cn (X. Xiao), john.ringwood@mu.ie (J.V. Ringwood).

https://doi.org/10.1016/j.renene.2024.121974
Received 16 January 2024; Received in revised form 14 November 2024; Accepted 20 November 2024
Available online 28 November 2024

pseudo-spectral (PS) method adopts a frequency-domain discretization, using Fourier series, to represent control trajectories and combines them with time-domain constraints to solve the control problem [10], which is a particularly suitable for the oscillating nature of WECs. The PS technique has been applied in a number of co-design studies, including WecOptTool, a co-design toolbox [11]. See Section 3 for a detailed description of current co-design options. Nevertheless, the need for optimization remains, and there exists considerable scope for acceleration in computation; the WEC community still needs a faster method, not only two or three times faster but orders of magnitude faster. As a prime example, the concurrent (co-design) optimization of array layout and *heterogeneous* device geometry optimization [12] presents a very challenging computational problem.

In this article, an ultra-fast optimal control performance evaluator is proposed, with MPC and PS (implemented using WecOptTool) being the benchmarks. The method is based on a wave-by-wave representation [13], which is common in wave analysis but novel in the WEC control context. By splitting the continuous long-term wave excitation force (WEF) into individual wave processes, the calculation of average power can be considerably simplified with this method termed the 'WbW' (wave-by-wave) method. First, an analytical optimal control solution, under a maximum stroke, during each individual wave of the WEF, is derived and then combined with the joint distribution of WEF amplitude and period. In this way, the need for iterative optimization is eliminated and the average power can be calculated hundreds of times faster than PS or MPC. Then, the method is generalized by combining PS and the wave-by-wave representation to address the PTO force constraint, and this second evolution is several times faster than the original PS. Finally, it will be shown that the WbW method can maintain the evaluation fidelity and arrive at the same co-design result as PS. However, the proposed method is intended purely for use in an off-line control co-design context, and is not intended for use as a real-time controller. Nevertheless, it may be possible to extend the control technique for real-time use, but this is the subject of a future study.

The contributions of this study are as follows. First, a powerful co-design tool to evaluate the optimal control performance of WECs is proposed. Second, an analytical optimal control solution is derived for individual waves of the WEF under a maximum stroke. Third, the possibilities following the WbW idea are developed, with the underlying mechanisms analysed in detail. Finally, this study marks the first time that the joint distribution of individual wave amplitude and period is combined with optimal control of WECs, which can provide insights for future research.

The remainder of this article is organized as follows. The WEC system model is introduced in Section 2, and existing control options for co-design are reviewed in Section 3. The WbW method is proposed in Section 4, and the validation of its fidelity and co-design result is presented in Section 5.

2. WEC system model

The schematic of a typical WEC is shown in Fig. 1. The body oscillates in heave when excited by waves and is linked to a PTO system. As commonly assumed in fundamental studies on WEC control, the PTO is regarded as an ideal actuator that produces the desired force issued by the controller.

2.1. Model of the body

The equation of motion in the frequency domain can be described [14] by

$$\left[j\omega(M + M_{\mathrm{a}}(\omega)) + (R_0 + R_{\mathrm{a}}(\omega)) + \frac{K}{j\omega}\right] V(j\omega) = W(j\omega) + U(j\omega), \tag{1}$$

where $j = \sqrt{-1}$, ω is the angular frequency, V, W, U are the body velocity, WEF, and PTO force, M, M_{a}, R_{a}, K, R_0 are the body mass, added mass, radiation damping, restoring force coefficient, and linearized damping for mechanical friction and viscous forces, respectively.

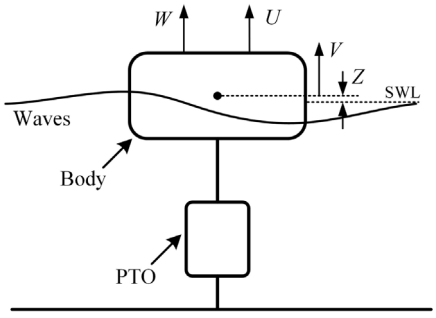

Fig. 1. Schematic of a typical WEC system. SWL: still water level.

The corresponding time-domain equation is

$$(M + M_\infty)\ddot{z}(t) + R_0\dot{z}(t) + \int_{-\infty}^{t} k_{\mathrm{r}}(t-\tau)\dot{z}(\tau)d\tau + Kz(t) = w(t) + u(t), \tag{2}$$

where t is continuous time, z, $\dot{z}$, and $\ddot{z}$ are the body position, velocity, and acceleration, w and u are the WEF and PTO force, M_∞ is the infinite-frequency added mass, and $k_{\mathrm{r}} = \mathcal{F}^{-1}\{R_a(\omega) + j\omega(M_a(\omega) - M_\infty)\}$ is the retardation function with $\mathcal{F}^{-1}$ denoting the inverse Fourier transform. The convolution term can be described as the output of the following system

$$\begin{aligned}\dot{\xi}(t) &= A_{\mathrm{r}}\xi(t) + B_{\mathrm{r}}\dot{z}(t)\\ \int_{-\infty}^{t} k_{\mathrm{r}}(t-\tau)\dot{z}(\tau)d\tau &\approx C_{\mathrm{r}}\xi(t),\end{aligned} \tag{3}$$

where $\xi \in \mathbb{R}^n$ is the radiation state, and $A_{\mathrm{r}}, B_{\mathrm{r}}, C_{\mathrm{r}}$ are the system matrices. Now, the overall WEC system can be expressed in a state-space form

$$\dot{x}(t) = Ax(t) + Bu(t) + Bw(t), \tag{4}$$

where $x = [\dot{z}, z, \xi^{\mathrm{T}}]^{\mathrm{T}} \in \mathbb{R}^{n+2}$ is the augmented state, and the matrices A and B are

$$A = \begin{bmatrix} -\frac{R_0}{M+M_\infty} & -\frac{K}{M+M_\infty} & -\frac{C_{\mathrm{r}}}{M+M_\infty} \\ 1 & 0 & 0_{1\times n} \\ B_{\mathrm{r}} & 0_{n\times 1} & A_{\mathrm{r}} \end{bmatrix}, B = \begin{bmatrix} \frac{1}{M+M_\infty} \\ 0 \\ 0_{n\times 1} \end{bmatrix}. \tag{5}$$

2.2. Model of the waves

A sea state is typically described by a significant wave height H_{s} and a peak period T_{p}. In this study, the following Bretschneider model is used

$$S(\omega) = \frac{5}{16}\frac{\omega_{\mathrm{p}}^4}{\omega^5}H_{\mathrm{s}}^2 \exp\left\{-\frac{5\omega_{\mathrm{p}}^4}{4\omega^4}\right\}, \tag{6}$$

where $S(\omega)$ is the energy spectrum, and $\omega_{\mathrm{p}} = 2\pi/T_{\mathrm{p}}$ is the peak frequency.

To generate a wave elevation signal from the spectrum, so as to assess the control performance, following the widely-used technique based on Fourier series [9], one can first determine a series of frequency points $n_1\omega_0, (n_1+1)\omega_0, \ldots, n_2\omega_0$ that covers the frequency range of $S(\omega)$, where ω_0 is the fundamental frequency, and then establish the following Fourier series

$$\eta(t) = \sum_{i=n_1}^{n_2} A_i \cos\left(i\omega_0 t + \phi_i\right), \tag{7}$$

where A_i and ϕ_i are the amplitude and phase of the ith component. The amplitudes are calculated as

$$A_i = \sqrt{2S(i\omega_0)\omega_0}, \quad i = n_1, \ldots, n_2, \tag{8}$$

while the phases $\phi_{n_1}, \dots, \phi_{n_2}$ are usually set to be artificial random variables independent and uniformly distributed over $[0, 2\pi]$ so that different wave signals can be generated from the same spectrum by shuffling the phases [9]. Accordingly, the time-domain WEF is

$$w(t) = \sum_{i=n_1}^{n_2} |F_e(ji\omega_0)| A_i \cos\left(i\omega_0 t + \phi_i + \angle F_e(ji\omega_0)\right), \tag{9}$$

where F_e is the (complex) excitation coefficients of the body, and $|\cdot|$ and $\angle\cdot$ denote the complex modulus and angle. Note that $\eta(t)$ and $w(t)$ are periodic with a period of $T = 2\pi/\omega_0$. Also note that $\eta(t)$ in Eq. (7) and $w(t)$ in (9) are linked with a linear, non-causal system ('wave-to-force' system); since Eq. (9) is directly generated from the frequency domain, it is, in fact, the steady-state output of that system, without any transients.

3. Control options for co-design

3.1. Linear controllers and variations

Linear controllers form the simplest choice for co-design. Conventional damping and reactive controllers are purely feedback, easy to implement, but not optimal under irregular waves. Panchromatic complex conjugate (CC) control achieves the unconstrained optimum, which is non-causal, and the linear time-invariant controller (LiTeCon) [15] can address the position constraint, although conservatively. The advantage of using linear controllers for co-design is that their average power can be directly calculated in the frequency domain offline [16,17], regardless of whether they require wave prediction in real-time implementation. Some other pseudo-linear approaches for co-design have also been reported. In [18,19], a linear controller is used, but the performance is evaluated in the time domain, where only the energy contributed by the trajectory within the constraints is included in the result. The controller is still not constraint-aware and the result cannot reflect the constrained optimum. Alternatively, in a recent project targeting the co-design of heterogeneous WEC arrays [20], the optimal control within a maximum control force and with positive power is solved using Pontryagin's principle. The controller switches between a linear, singular-arc law and a bang–bang control, and can be efficiently simulated in the time domain. Nevertheless, the controller is designed for regular waves, and the maximum stroke, as one of the most critical constraints of a WEC, cannot be handled.

From this category of 'simple' WEC controllers, CC control is chosen as the first benchmark, since it gives an upper bound for what a given geometry can achieve. Under CC control, (frequency-domain) optimal velocity satisfies

$$V(j\omega) = \frac{W(j\omega)}{2(R_0 + R_a(\omega))}. \tag{10}$$

The average power converted equals the captured wave power minus the power loss

$$\bar{P}(\omega) = \frac{1}{2}\mathrm{Re}\{W(j\omega)\hat{V}(j\omega) - V(j\omega)\hat{V}(j\omega)(R_0 + R_a(\omega))\}, \tag{11}$$

where Re denotes the real part, and $\hat{V}$ denotes the complex conjugate of V. Combining Eqs. (8)–(11), the average power can be calculated as

$$\bar{P} = \sum_{i=n_1}^{n_2} \frac{|F_e(ji\omega_0)|^2 S(i\omega_0)\omega_0}{4(R_0 + R_a(i\omega_0))}, \tag{12}$$

and this can be computed without deriving a real-time CC control law.

3.2. MPC (Receding-horizon, time-domain-discretized control)

Compared to linear control, MPC offers a unified framework for constraint handling and represents the optimal constrained performance [4,7]. For example, MPC-based co-design is adopted in [21] to study the effects of various mechanical and electrical constraints. However, computation remains the biggest obstacle to its application.

In this study, MPC refers to the receding-horizon, time-discretized MPC, with an energy-maximizing performance objective for WEC control [4], and is taken as the second benchmark. The MPC algorithm in [8] that falls into this category is used. Two critical constraints are considered: The maximum stroke Z_m and the maximum PTO force U_m. First, the continuous-time model is discretized into

$$x[k+1] = A_d x[k] + B_d u[k] + B_d w[k], \tag{13}$$

where k is the discrete time index with a sampling time of T_s, and A_d and B_d are the discrete-system matrices; using zero-order-hold discretization, there are $A_d = \exp\{AT_s\}$ and $B_d = A^{-1}(A_d - I)B$ with I being the identity matrix. At each step of MPC, a control sequence $\bar{u}_0, \dots, \bar{u}_{N-1}$ starting from the current state $x[k]$ and going through the predicted WEFs $w[k], \dots, w[k+N-1]$ during a prediction horizon N is solved, such that it maximizes the extracted energy during the prediction horizon, while satisfying the constraints. This optimization problem can be expressed as

$$\begin{aligned}
\max_{\bar{u}_0,\dots,\bar{u}_{N-1}} \quad & \bar{E} = \sum_{i=0}^{N-1} \bar{R}_i, \\
\text{s.t.} \quad & \bar{R}_i = -\frac{1}{2} T_s C_1 (\bar{x}_i + \bar{x}_{i+1}) \bar{u}_i, \quad i = 0, \dots, N-1 \\
& \bar{x}_{i+1} = A_d \bar{x}_i + B_d \bar{u}_i + B_d \bar{w}_i, \quad i = 0, \dots, N-1 \\
& -Z_m \le C_2 \bar{x}_i \le Z_m, \quad i = 1, \dots, N \\
& -U_m \le \bar{u}_i \le U_m, \quad i = 0, \dots, N-1 \\
& \bar{x}_0 = x[k], \quad \bar{w}_i = w[k+i], \quad i = 0, \dots, N-1,
\end{aligned} \tag{14}$$

where C_1, C_2 are row vectors defined such that $C_1 x = \dot{z}$, $C_2 x = z$, $\bar{R}_i$ is the extracted energy between the ith and $(i+1)$th instants and is calculated by trapezoidal integral, and $\bar{E}$ is the total energy output. This optimization is a quadratic program (QP). Note that although there is no theoretical guarantee for its convexity, in practice, realistic WEC parameters usually correspond to a convex QP [8], and there are techniques to convexify the problem with additional penalty terms [22]. After the optimal control sequence is solved, only its first move $\bar{u}_0$ will be applied, and the above process is repeated at the next step. In general, simulation of an MPC-controlled WEC system needs to solve a series of 'local' optimization problems. The tuning strategy for the MPC parameters is given in Appendix.

Note that since the goal is control evaluation rather than real-time control, a 'global' version of MPC remains another alternative, which solves a single optimal control problem over the entire operating horizon. However, it is shown in the Appendix that global MPC is computationally less preferable, due to its high optimization dimension, and is therefore not considered in the remainder of this study.

3.3. Pseudo-spectral methods (Global horizon, frequency-domain-discretized control)

To reduce the computational burden, the optimal control problem can be discretized in a different way. A preliminary method can be found in [23,24], where the system trajectory over the entire operating horizon is represented by Fourier series, and the original constraints are approximated with 2-norm constraints on Fourier coefficients, but this treatment remains conservative [25]. The PS method marks an important development in this direction. PS uses a wide range of frequency components and handles the constraints at a series of time instants, or 'colocation' points [10]. Compared with MPC, the PS formulation suits the oscillating nature of WEC systems very well and has seen a number of applications in co-design [5,11,26–28]. More recently, a novel parameterization method, based on moments, has been developed, which has the advantage of a guaranteed unique global solution for nonlinear problems [29].

The global PS method, implemented using WecOptTool [11], is taken as the third benchmark. Using the Fourier series, the WEF can be described by

$$w(t) = \sum_{i=1}^{m/2} W_{ai}\cos(i\omega_0 t) + W_{bi}\sin(i\omega_0 t), \tag{15}$$

where W_{ai} and W_{bi} are the coefficients for sin and cos, and m is the number of components. Comparing Eqs. (9) and (15), one can easily see that Eq. (9) includes frequency points $\omega_0, 2\omega_0, \dots, (m/2)\omega_0$, containing additional low- and high-frequency components outside the frequency range $n_1\omega_0, (n_1+1)\omega_0, \dots, n_2\omega_0$ in Eq. (15) (m should be chosen such that $m/2 > n_2$). Hence, let $W_i = F_e(ji\omega_0)A_i e^{j\phi_i}$, so that $W_{ai} = |W_i|\cos(\angle W_i)$ and $W_{bi} = -|W_i|\sin(\angle W_i)$ for $i = n_1, \dots, n_2$, and $W_{ai} = W_{bi} = 0$ for $i < n_1$ and $i > n_2$. However, the sin and cos coefficients for $\dot{z}$, z and u are generally non-zero when $i < n_1$ and $i > n_2$. This is because, under hard constraints, the system variables include additional low- and high-frequency components. Define the following row vector

$$\vec{\Phi}(t) = \left[\cos(\omega_0 t), \sin(\omega_0 t), \dots, \cos\left(\frac{m}{2}\omega_0 t\right), \sin\left(\frac{m}{2}\omega_0 t\right)\right]. \tag{16}$$

Then, the system variables can be expressed in a vector form as $w(t) = \vec{\Phi}(t)\vec{W}$, $\dot{z}(t) = \vec{\Phi}(t)\vec{V}$, $z(t) = \vec{\Phi}(t)\vec{Z}$, and $u(t) = \vec{\Phi}(t)\vec{U}$, where $\vec{W}$, $\vec{V}$, $\vec{U}$, and $\vec{Z}$ are row vectors containing the corresponding amplitudes. The system equation can be expressed as

$$G\vec{V} = \vec{W} + \vec{U}, \tag{17}$$

where G is the (invertible) system matrix as derived in [10]. The constraints are imposed on a series of time instants $t_0, t_1, \dots, t_{N_c}$ uniformly distributed over $[0, T]$, with $(N_c + 1)$ being the number of collocation points. Further defining the matrix $\Phi = [\vec{\Phi}^{\mathrm{T}}(t_0), \dots, \vec{\Phi}^{\mathrm{T}}(t_{N_c})]^{\mathrm{T}}$, the optimization problem can be formulated as the maximization of extracted energy within constraints

$$\begin{aligned} \max_{\vec{U}} \quad & -\frac{T}{2}\vec{U}^{\mathrm{T}}\vec{V} \\ \text{s.t.} \quad & -U_m \le \Phi\vec{U} \le U_m, \\ & -Z_m \le \Phi\vec{Z} \le Z_m. \end{aligned} \tag{18}$$

This problem is also a QP, but different from MPC in that it is a single, global, optimization. The tuning strategy for the PS control parameters is given in Appendix.

Note that PS control can also be developed into a receding-horizon version, for real-time control. However, going from global PS control to receding-horizon PS control entails additional complexities, compared to the MPC case, and is unlikely to result in significant computational saving. If Fourier series is used as the basis function, a windowing function is needed to handle non-periodicity, and the control has a long horizon length requirement [30], additional time-frequency domain transformation, and more control parameters to tune [31]. Alternatively, other more complicated basis functions are needed [32]. Hence, receding-horizon PS control is not considered in this study. To the best of the authors' knowledge, all existing PS-based control co-design works are based on global PS (e.g., [5,11,26–28]) which, therefore, is the ideal benchmark for this study.

Finally, note that co-design requires evaluation of the long-term expected power generation of a given sea state. This is achieved in two stages: First, for each (periodic) WEF signal, simulated using Eq. (9), the steady-state control performance is calculated. This means that the effect of the initial state (the transients) should be eliminated. The PS control described above focuses exclusively on the steady-state control trajectories. For MPC, however, additional procedures, such as discarding the initial phase of the MPC simulation, are needed; see the Appendix for details. Second, multiple realizations of the WEF signal are simulated by shuffling the phases in Eq. (9) [9], the corresponding (steady-state) performance is evaluated, and then the mean value is taken as the expectation of long-term power generation.

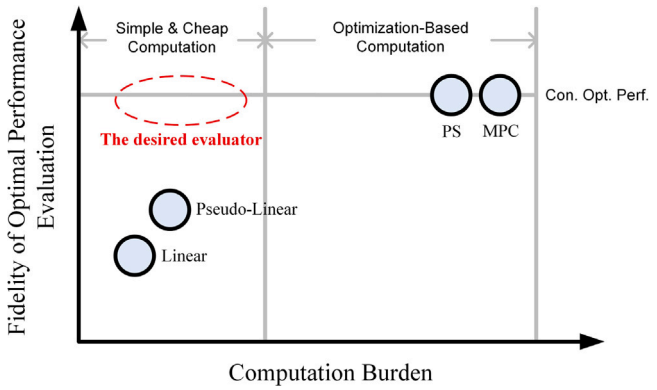

Fig. 2. The fidelity-computation relationship of the controller continuum (for indicative use, not to scale). Con. Opt. Perf.: constrained optimal performance.

3.4. The fidelity-computation map

The control performance evaluation approaches described above show different features in fulfilling the goal of optimal control performance evaluation. The linear or pseudo-linear methods are fast but are, in general, non-optimal and/or non-constrained; their result deviates from the real constrained optimum. MPC is optimal but computationally demanding. This predicament constitutes the fidelity-computation dilemma: Greater computation effort is needed for a more accurate optimal constrained evaluation. In this sense, PS is an improvement on MPC, since optimality (within the fidelity of the Fourier representation) is maintained with faster computation, though not significantly faster. The fidelity-computation characteristics of these methods are shown conceptually by the blue balls in Fig. 2, with the current objective being to propose an *evaluator* that is at the same time very accurate and very fast, as shown by the red circle in Fig. 2.

3.5. A brief comparison of benchmarks

Here, an illustrative example of CC, MPC, and PS is presented. The wave parameters are $H_s = 1$ m, $T_p = 6$ s, and $\omega_0 = 0.01 \times 2\pi$ rad/s, so the generated wave signal has a period of 100 s. The body is a vertical cylinder with a radius of 2 m and a draught of 2 m, whose hydrodynamic parameters are calculated using NEMOH [33]. In this study, for research purpose, the damping R_0 is set to be proportional to the square of body radius with a coefficient of 0.5 kNs/m^3. The maximum stroke is set to $Z_m = 1$ m. CC control follows Eq. (12), while the control parameters of MPC and PS are tuned as in Appendix. MPC utilizes the MATLAB function 'quadprog' to solve the quadratic programs; the MPC simulation involves 1120 simulation steps and, at each step, a 60-dimensional quadratic program with 240 inequality constraints needs to be solved. PS is implemented using the WecOptTool [11], involving a single optimization with 114 frequency components, 458 optimization variables, 229 equality constraints, and 1824 inequality constraints. The results are shown in Fig. 3.

It can be seen that MPC and PS achieve almost the same result. The evaluated average power, with eight phase realizations, are 10.15 and 10.21 kW, respectively, which are very close, representing the optimal constrained performance for the current wave signal. On the other hand, CC reaches 14.52 kW, but the position is not constrained, so this power cannot reflect the performance of a realistic WEC. The numerical testing is performed on an i7-13700H @2.40 GHz processor, and the average computation times are 8.2 s for MPC and 6.4 s for PS, so PS is slightly faster, but their speeds are still of the same order. Note that this is only one phase realization, and the above process should be repeated multiple times to get statistically significant results.

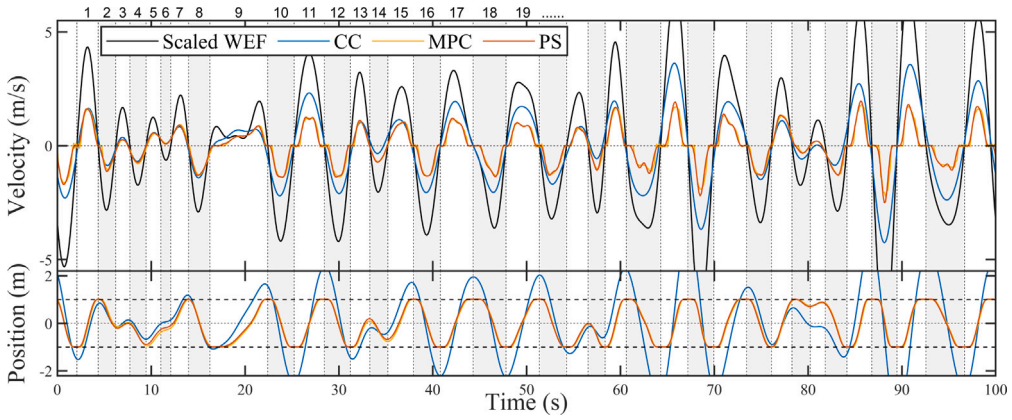

Fig. 3. The control trajectories of CC, MPC, and PS. The WEF signal can be decomposed into individual half waves, each is marked with an index.

4. A new optimal control performance evaluator

4.1. The wave-by-wave idea

To circumvent the need for iterative optimization, the optimal position-constrained profiles in Fig. 3 is re-examined. In fact, it can be seen that the system trajectories during each half wave, i.e., each positive or negative half cycle (each 'crest' or 'trough') of the WEF, shows a clear characteristic:

- For small half waves, the constraint is inactive, and the velocity is typically 'in phase' with the WEF, namely, they have the same sign, the same peak time, and similar waveforms.
- For large half waves, the constraint is active, and the system typically shows a 'latching' behaviour; during the starting and ending phases, the velocity is zero and the position is kept at its maximum; during the mid-phase, the body moves from one of its maximal positions to the other, and the velocity profile is also 'in phase' with the WEF.

This clear relationship between the WEF and optimal velocity can be exploited, i.e., used as *a priori* knowledge for the control solution. Specifically, it is assumed, as in [34], that:

- A1: The radiation convolution force can be represented using a locally constant linear damping term (to be described later),

and it is further assumed, from the two observations above, that:

- A2: During each half wave, the body *always* moves in the same direction as the WEF, either freely, i.e., without reaching the maximum positions (the constraint is inactive), or from one maximum position to the other (the constraint is active).

Note that A1 and A2 naturally correspond to the well-known optimal control condition (impedance-matching condition) under regular waves with no constraints, and they are here extended to address constrained cases under irregular waves. With these assumptions, each half wave of the WEF corresponds to an independent process, and the energy maximization problem of the long-term wave process can be transferred into the problem of solving, for each half wave, an optimal velocity profile that maximizes the energy during this half wave.

This is the fundamental basis of the WbW (wave-by-wave) method: To decompose the WEF signal, according to its zero-crossing points, into independent half waves and process each one separately. This decomposition is illustrated in Fig. 3.

4.2. Half-wave optimal control

The benefit of assuming half-wave independence is that the optimal control solution becomes very simplified. To show this, the Pontryagin's method is used for analysis. Consider a positive half cycle (a 'crest') of the WEF $w(t)$ during a time interval $[0, D]$

$$w(t) \geq 0, \quad t \in [0, D]. \tag{19}$$

The optimal velocity profile is the desired solution, so the system state is the position z and the control is the velocity v. The system equation is

$$\dot{z}(t) = v(t), \tag{20}$$

while the control objective is to maximize the converted energy

$$\int_0^D \left(w(t)v(t) - R_{\text{local}} v^2(t) \right) dt. \tag{21}$$

Note that: (1) The energy is expressed as the difference between the energy captured from the waves and the energy lost by the body, similar to Eq. (11), and this expression avoids the PTO force term. (2) Originally, the radiation effect is represented by the frequency-dependent damping $R_a(\omega)$ or the radiation kernel $k_r(t)$ in the time domain, but here, a 'local' frequency, similar to the 'instantaneous' frequency in the Simple and Effective controller [34] is used. The local frequency is identified as $\omega = \pi / D$, so that the system damping can be determined as

$$R_{\text{local}} = R_0 + R_a \left(\frac{\pi}{D} \right). \tag{22}$$

It is easy to see that R_{local} is consistent with the exact model under regular waves while, under irregular waves, it remains an effective approximation [34].

The control solution depends on whether the position constraint is inactive or active. In the first case, the control is unconstrained. The Hamiltonian is

$$H(w(t), v(t), p(t)) = w(t)v(t) - R_{\text{local}} v^2(t) + p(t)v(t), \tag{23}$$

where $p(t)$ is the covariant. The optimal condition is

$$\frac{\partial H}{\partial v} = -2R_{\text{local}} v(t) + w(t) + p(t) = 0, \tag{24}$$

In addition to Eq. (20), the covariant satisfies

$$\frac{\partial H}{\partial z} = -\dot{p}(t) = 0. \tag{25}$$

Since the terminal time is fixed and the terminal state (position) is unconstrained, have

$$p(D) = 0. \tag{26}$$

So, $p(t) \equiv p(D) = 0$ for $t \in [0, D]$, and

$$v^*(t) = \frac{w(t)}{2R_{\text{local}}}. \tag{27}$$

This is consistent with the well-known optimal condition: The velocity is proportional to the WEF with a coefficient of $2R_{\text{local}}$. Note that since $w(t) \geq 0$, it is clear that there is $v(t) \geq 0$ as well.

For the second case, the body moves unidirectionally from the negative position limit to the positive one, so

$$v(t) \geq 0, \quad t \in [0, D]. \tag{28}$$

According to Pontryagin's maximum principle, condition (24) is now replaced by

$$v^*(t) = \underset{v \geq 0}{\text{argmax}}\, H(w(t), v, p(t)). \tag{29}$$

Since the terminal state (position) is now fixed, there is no boundary condition for $p(t)$. Recall that $\dot{p}(t) = 0$, so let $p(t) \equiv -P, t \in [0, D]$ with P constant. It is easy to see, from Eqs. (23) (28) (29), that the optimal velocity satisfies

$$v^*(t) = \begin{cases} \frac{(w(t)-P)}{2R_{\text{local}}}, & \text{if} \quad w(t) - P > 0 \\ 0, & \text{if} \quad w(t) - P \leq 0. \end{cases} \tag{30}$$

Since the total distance the body moves is $2Z_{\text{m}}$, P must satisfy

$$\int_0^D v^*(t)dt = 2Z_{\text{m}}. \tag{31}$$

The optimal velocity profile can be solved by combining Eqs. (30) and (31). This solution has the following features: When the WEF is below a threshold P, the velocity is maintained at zero; otherwise, the velocity is proportional to the difference between the WEF and the threshold, also with a coefficient of $2R_{\text{local}}$. This is exactly the latching behaviour observed from Fig. 3.

4.3. Analytical solution

The solution in Section 4.2 still depends on the specific shape of the WEF. To proceed to an analytical solution, $w(t)$ is approximated with a sinusoidal function, namely,

$$w(t) = W \sin\left(\frac{\pi}{D}t\right), \quad t \in [0, D]. \tag{32}$$

When the position constraint is active, let $\alpha = \arcsin(P/W)/\pi$, there is $\alpha \in [0, 0.5]$, and the optimal velocity is

$$v^*(t) = \begin{cases} \frac{W}{2R_{\text{local}}}\left(\sin\left(\frac{\pi}{D}t\right) - \sin(\alpha\pi)\right) & , t \in [\alpha D, (1-\alpha)D] \\ 0 & , \text{otherwise}. \end{cases} \tag{33}$$

Then, the total distance the body moves is

$$\int_0^D v^*(t)dt = \frac{WD}{2R_{\text{local}}}\left[(2\alpha - 1)\sin(\alpha\pi) + \frac{2}{\pi}\cos(\alpha\pi)\right] = \frac{WD}{2R_{\text{local}}} f(\alpha). \tag{34}$$

It is easy to see that, when $\alpha = 0$, the displacement reaches its maximum. If this maximum does not exceed the position constraint, i.e., $f(0)WD/(2R_{\text{local}}) = WD/(\pi R_{\text{local}}) \leq 2Z_{\text{m}}$, the constraint is deemed to be inactive. Otherwise, the constraint is active, and α should satisfy $WDf(\alpha)/(2R_{\text{local}}) = 2Z_{\text{m}}$. In summary,

$$\alpha = \begin{cases} f^{-1}\left(\frac{4R_{\text{local}}Z_{\text{m}}}{WD}\right), & \text{if} \quad \frac{WD}{\pi R_{\text{local}}} > 2Z_{\text{m}} \\ 0, & \text{if} \quad \frac{WD}{\pi R_{\text{local}}} \leq 2Z_{\text{m}}, \end{cases} \tag{35}$$

where f^{-1} is the inverse function of f, and it is easy to verify that f has a unique inverse when $\alpha \in [0, 0.5]$. The variable α can be viewed as a constraint index, for which a higher value corresponds to a tighter constraint. Finally, the energy E during the half wave is

$$E = E(W, D) = \frac{W^2 D}{8R_{\text{local}}}\left[1 - 2\alpha + \frac{1}{\pi}\sin(2\pi\alpha) + (4\alpha - 2)\sin^2(\alpha\pi)\right]. \tag{36}$$

Additionally, the system trajectory, corresponding to the half-wave control solution, is illustrated in Fig. 4(a), where the PTO force profile is calculated from the optimal velocity using the local system model. It can be seen that the 'latching' behaviour of the control solution gives a discontinuous PTO force profile. However, note that the aim here is to evaluate the control performance, rather than to develop a real-time controller, so the smoothness of control action is not the primary concern. In real-time control (possibly following a co-design optimization stage), MPC or receding-horizon PS controllers can be applied to achieve more smooth control actions.

In summary, by adopting a sinusoidal approximation, the half wave waveform is reduced to two characteristic parameters, i.e., the amplitude W and the duration D (half the period), and the energy can be analytically calculated using Eqs. (35) and (36). As a special case, when unconstrained, $\alpha = 0$, and the average power is $E/D = W^2/(8R_{\text{local}})$, which is consistent with the optimal condition [35].

4.4. Average power calculation

With the very simple energy function described by Eqs. (35) and (36), it is straightforward to calculate the average power: A number of WEF signals are generated using Eq. (9), the half-wave parameter samples $\{W_i, D_i\}_{i=1}^{N_s}$, with N_s being the number of half waves, are recorded, the energy for each sample are calculated, and finally, the results are averaged. The average power can be expressed as

$$\bar{P} = \frac{\sum_{i=1}^{N_s} E(W_i, D_i)}{\sum_{i=1}^{N_s} D_i}. \tag{37}$$

This straightforward WbW calculation process consists of two fundamental steps: (1) Get the W–D distribution and (2) calculate the optimal energy for each W–D sample. In this sense, the above method is termed WG/A (Wave Generation with Analytical solution).

Alternatively, an analytic model of the W–D joint distribution, such as the Longuet-Higgins (LH) model [36], can be employed for the first step. Denote the spectrum of the WEF as $S_{\text{wf}}(\omega)$, with $S_{\text{wf}}(\omega) = |F_{\text{e}}(j\omega)|^2 S(\omega)$, and define

$$m_n = \int_0^\infty \omega^n S_{\text{wf}}(\omega)d\omega, \tag{38}$$

$$\nu = \frac{m_0 m_2}{m_1^2} - 1, \tag{39}$$

$$c_{\text{LH}} = \frac{1}{8}(2\pi)^{-\frac{1}{2}}\nu^{-1}\left(1 + (1+\nu^2)^{-\frac{1}{2}}\right)^{-1}, \tag{40}$$

and then, the joint density $p_{\text{LH}}(W, D)$ is

$$p_{\text{LH}}(W, D) = c_{\text{LH}}\left(\frac{W}{D}\right)^2 \exp\left\{-\frac{W}{8}\left(1 + \nu^{-2}(1 - D^{-1})^2\right)\right\}. \tag{41}$$

Now, the average power can be calculated by integrating over the probability distribution

$$\bar{P} = \frac{\iint p_{\text{LH}}(W, D)E(W, D)dW\,dD}{\iint p_{\text{LH}}(W, D)DdW\,dD}. \tag{42}$$

This method is termed LH/A (LH model with Analytical solution). However, unlike the WG approach with no assumption on the wave spectrum, the LH model is based on a narrow-banded assumption and cannot represent the full shape of the spectrum, so may be prone to deviate from the real distribution [37], and this will be tested in Section 5.1.3.

An illustration of the LH/A method, based on the case study in Section 3.5, is given in Fig. 4(b) and (c). The WAFO toolbox [38] is used for the basic probability calculations. It can be seen that the half-wave amplitude and duration of the WEF have a clear correlation; on the other hand, the energy function shows that a larger and longer wave generally corresponds to higher energy and tighter constraints, although they are also affected by the frequency-dependent radiation damping. The average power estimated by LH/A is 9.98 kW, while recall that the average results obtained by MPC and PS are 10.15 and 10.21 kW, respectively; this level of fidelity is already sufficient for a quick evaluation of the WEC design parameters and their dependence on the control. The computation time is about 0.01 s, thousands of times faster than MPC (8 × 8.2 s) and PS (8 × 6.4 s) since no iterative optimization is required for LH/A. This result already shows the computational advantage of the WbW method.

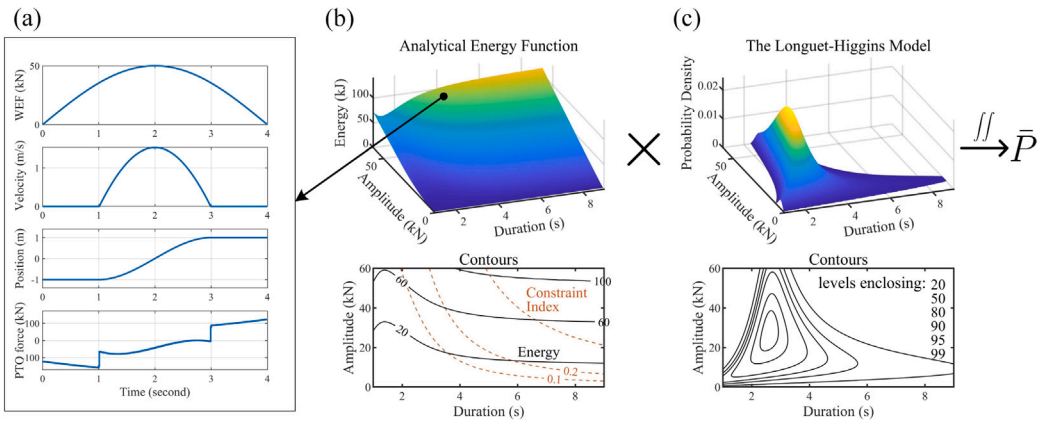

Fig. 4. An illustration of the LH/A method. (a) The half-wave optimal control profile in Section 4.3. (b) The surface and contours of the half-wave energy function Eq. (36) and the contours of the constraint index Eq. (35). With the distribution and energy function, the average power can be calculated with Eq. (42). (c) The surface and contours (enclosing 20%, 50%, …, 99% probability) of the joint density of half-wave amplitude and duration of the WEF based on the LH model.

4.5. The generalized WbW method

The above analytical solution has focused only on the constraint of maximum stroke. For more general constraints, such as the maximum PTO force, no analytical solution exists, and one has to resort to a numerical solution. However, the idea of calculating the performance by regarding each half wave of the WEF as an independent process is still useful in attempting to generalize the original WbW method. Specifically, it is proposed that, for each W–D pair, the half-wave energy can be calculated by solving the optimal control problem for the corresponding regular wave case, namely, the regular wave with an amplitude of W and a period of $2D$, which can be achieved using PS control. Compared with the analytical energy function, the numerical method is slower, but compared with the original PS that addresses the complete evaluation horizon, it is significantly faster. This is due to the fact that, under regular waves, the number of sinusoidal components and the number of time instants to impose constraints are both very much reduced; in other words, the optimization problem contracts and can be solved rapidly. Hence, it is profitable to use PS control in a wave-by-wave manner. Finally, by combining the numerical solution with either a data distribution or an LH model, two further variations can be naturally obtained: WG/N and LH/N (Wave Generation or LH model with Numerical solution).

5. Case studies

5.1. Verification of wave-by-wave assumptions

Here, the initial focus is on the assumptions taken in the WbW method, including the use of local damping, the wave-by-wave independence, and the narrow-bandedness of the LH model. The studied body parameters are the same as in Section 3.5.

5.1.1. Exact radiation convolution vs. Local damping

The first test is to show how much evaluation error can be caused by using local damping instead of the exact radiation convolution. A W–D grid is considered and, for each grid point, the optimal half-wave energy is solved using (i) the regular-wave PS solution with an exact radiation kernel and (ii) the analytical energy function Eqs. (35) and (36) with local damping. This test is repeated by changing the maximum stroke Z_m and the constant system damping R_0, respectively. Note that R_0 is determined by the mechanical part of the WEC, and so can vary significantly across different devices. In this study, for research purposes, an intuitive assumption is taken in which R_0 is proportional to the device cross-sectional area, with a coefficient of 0.5 kN·s/m^3. The discrepancy is defined as the relative difference (percentage) between the results. The testing results, as well as the value of R_0 compared to the radiation damping, are shown in Fig. 5. It can be seen in each sub-figure that, when either the WEF amplitude W or duration D is large enough, the discrepancy occurs. This is because for a larger wave the constraint becomes active, and the dynamic process cannot be fully described by a fixed damping. Consequently, as the maximum stroke increases, the discrepancy-free region is expanded. Under different R_0 values, similar observations can be made, and the error resulting from local damping is generally below 5% under the original R_0 and further decreases to be less than 4% and 2% as R_0 increases. This is also reasonable, since as the constant part of the frequency-dependent damping increases, the variant part, corresponding to the memory effect of the radiation kernel that cannot be grasped by local damping, becomes less influential. In summary, using simple local damping can give a reasonably accurate evaluation result.

5.1.2. Coupled waves vs. Independent individual waves

The second study investigates how much power evaluation error can result from the assumption of wave-by-wave independence. A long-term WEF signal is first generated, and then the average power is calculated using (i) a PS solution that addresses the entire process and (ii) the WG/N method that calculates each half wave independently. This test is repeated for different values of H_s and T_p, and for each H_s–T_p point 16 phase realizations, and three different values of maximum stroke Z_m; the results are shown in Fig. 6. Although there is no clear relationship between the wave parameters and the discrepancy, it can be seen that the error is generally below 3%, and the maximum stroke setting does not have a significant impact on the discrepancy level. Hence, wave-by-wave independence is a reasonable and effective approximation for power evaluation.

5.1.3. Wave signal generation vs. LH model

The third study investigates whether the analytical LH model gives a result that is in accordance with the actual data distribution obtained from a Bretschneider spectrum. The body radius is 2 m and the draught is 2 m, the sea state parameters are H_s = 1 m and T_p = 6 s, and the results are shown in Fig. 7, which shows that the data distribution has faster decay at large durations, and its peak regions are more inclined towards small waves. This is due to the fact that the LH model is based on a narrow-banded assumption and uses only a few parameters of the WEF spectrum, so it cannot incorporate the full spectral shape [36,37]. On the other hand, while an exact distribution can be calculated numerically from the spectrum [39], such an approach has a considerable computational requirement, which runs counter to the intention of speeding up the evaluation process. Hence, only the WG and LH methods are further considered in this study, and the WG method is generally more reliable.

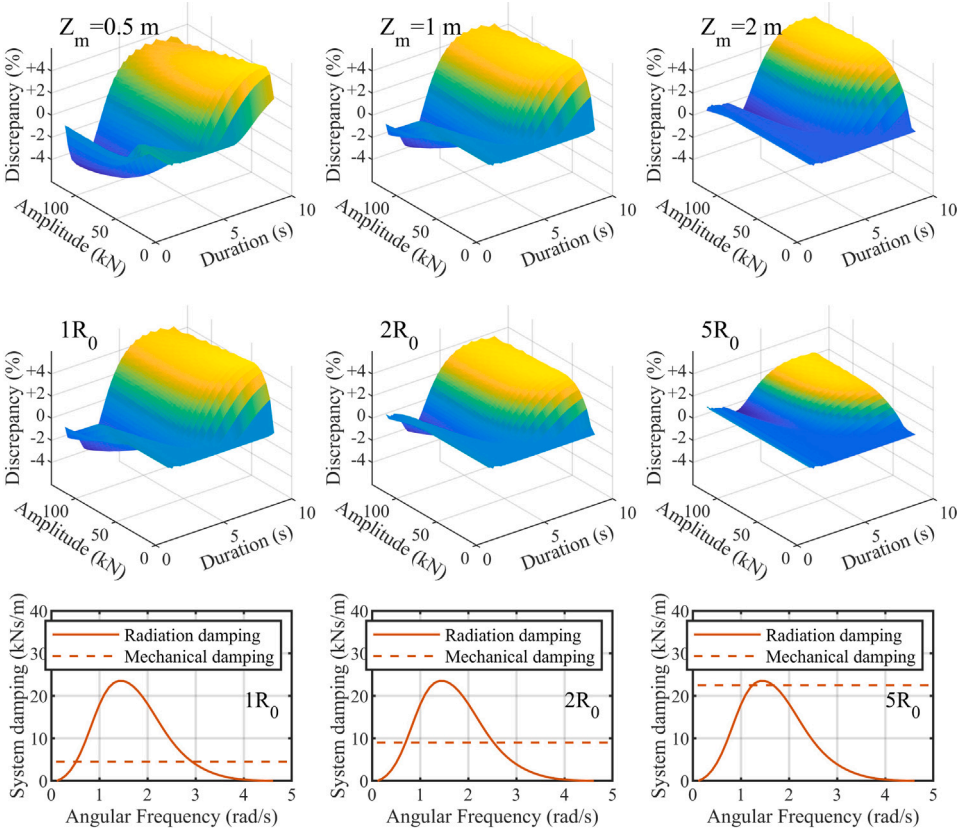

Fig. 5. Discrepancy of average power calculation between using the exact radiation convolution kernel and using a local radiation damping (body radius 3 m, draught 2 m). The values of R_0 and radiation damping are also illustrated.

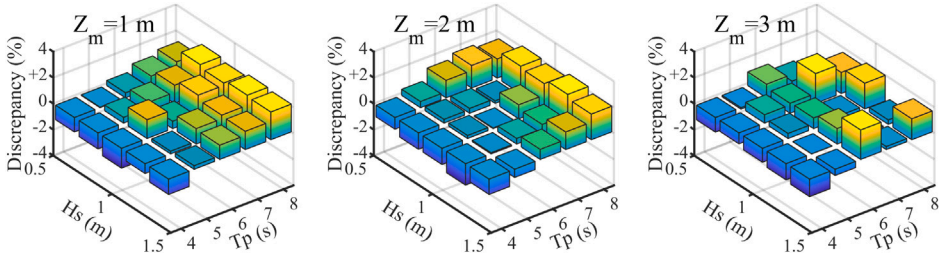

Fig. 6. Discrepancy of average power calculation between solving the entire process as a whole and solving each half wave independently (body radius 3 m, draught 2 m).

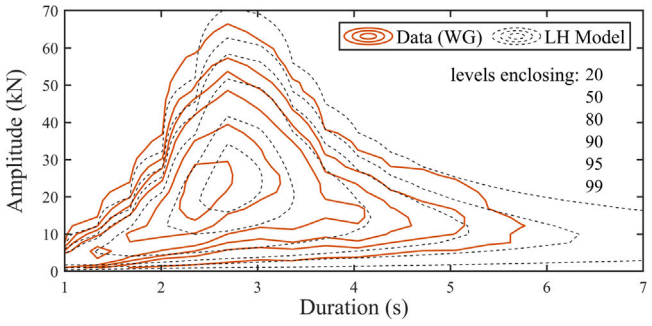

Fig. 7. Comparison between the WG method (data distribution) and LH model.

5.2. Comparison between the four variations of the WbW method

Now, the four variations of the WbW method: WG/A, LH/A, WG/N, and LH/N are compared to examine their evaluation fidelity and highlight their features. The four methods are used to estimate the average power of the WEC device, documented in Section 3.5, under a number of different sea states. The selected sea states come from real measured data of Wheat Island in the East China Sea [40]. The number of occurrences of different sea states is shown in Fig. 8 (left). From a wave energy perspective, a selected wave range is determined, which excludes too-small and too-large waves. The corresponding distribution of wave energy density, which is a linear function of $H_s^2 T_p$ [41], is shown in Fig. 8 (right). Then, nine representative sea states covering the selected range are now chosen, as also shown in Fig. 8 (right). The body radius is 2 m and the draught is 2 m; the maximum stroke is 1.5 m. The evaluation results of the four methods are compared to the full PS solution, which is the constrained optimum, and are shown in Fig. 9.

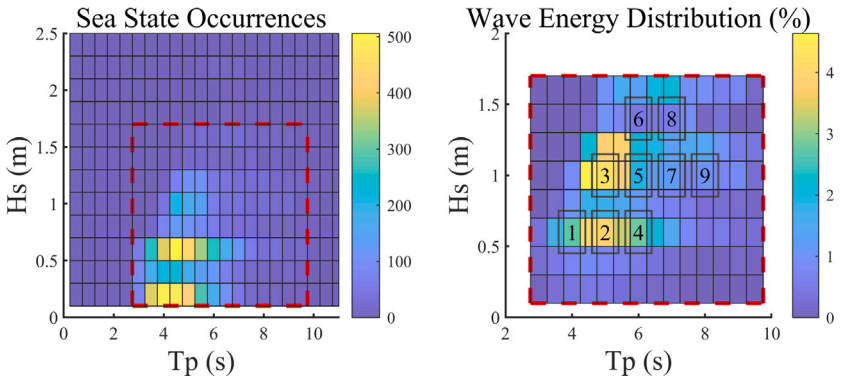

Fig. 8. Wave data of Wheat Island, East China Sea, 2021. Left: the number of occurrences of each sea state. Right: the wave energy distribution. The selected nine sea states are (H_s, T_p) = (0.6, 4), (0.6, 5), (1.0, 5), (0.6, 6), (1.0, 6), (1.4, 6), (1.0, 7), (1.4, 7), (1.0, 8), the units are (m) and (s), respectively.

The following two observations can be made. On the one hand, the results of the WG methods (WG/A and WG/N) are closer to PS than the LH methods (LH/A and LH/N), which exhibit a certain underestimation. This can be explained by the deviation of the LH model from the data distribution. On the other hand, either with WG or LH, the discrepancy between the analytical and numerical solutions (i.e., WG/A vs. WG/N, and LH/A vs. LH/N) is generally small. This means that the error caused by the LH distribution is the main factor affecting the evaluation fidelity, while the use of local damping has a smaller contribution to the power evaluation error.

The average computation times are shown in Fig. 10. It can be seen that MPC and PS have the heaviest computational burden while, in contrast, the computation times of the analytical WbW methods (WG/A and LH/A) are almost negligible. Note that LH/A is generally faster than WG/A, since when using an analytical energy function, the main computational load comes from the wave signal generation. However, both methods are already fast enough for co-design, so WG/A, with a more accurate evaluation, remains the better choice. On the other hand, the generalized WbW methods (WG/N and LH/N), although adopting a PS solver, are still much faster than the original PS. Hence, it can be concluded that the WbW method is hundreds of times faster than PS, under maximum stroke only (where WG/A is utilized), and several times faster than PS when a maximum PTO force is also included (where WG/N is utilized).

5.3. Comprehensive validation of evaluation fidelity

To fully validate the evaluation fidelity, four different cylindrical bodies with radii and draughts of (1,1), (2,1), (2,2), and (3,2) m are considered and denoted as Bodies 1–4; their parameters are listed in Table 1. The body size is chosen based on the fact that the dominant T_p of the sea area is 4–5 s, which corresponds to a wavelength range of 20–40 m, so the body diameter should not be too large compared to the wavelength. Since the maximum stroke and maximum PTO force are highly correlated with the device size, a 'maximum stroke factor', denoted as r_z, is defined as the ratio of Z_m to the body draught, and a 'maximum force factor', denoted as r_u, is defined as $U_m/(KZ_m)$. In this way, six constraint cases are tested, where $r_z = [0.75, 0.5]$ and $r_u = [\infty, 0.75, 0.5]$. The results are shown in Fig. 11. It can be seen that, for the force-unconstrained case ($r_u = \infty$), the accuracy of WG is higher than LH, and the evaluation error is limited to 5% by using WG and 6% by using LH. Similarly, when the PTO force constraint is introduced, the error of WG is below 5%, lower than LH, which is generally below 10%. Hence, the results confirms again that, in the WbW method, it is better to obtain the half-wave parameter distribution using WG rather than LH. The best choice is to use WG/A for the position constraint only and WG/N for general constraints, and the overall evaluation error is less than 5%.

Table 1
Parameters of the examined bodies.

Parameters	Body 1	Body 2	Body 3	Body 4
Radius (m)	1	2	2	3
Draught (m)	1	1	2	2
Resonant Frequency (rad/s)	2.51	2.21	1.78	1.66

5.4. Control co-design example

Finally, an application example of the proposed evaluator in WEC geometry control co-design. For simplicity, the design parameter is the size of the body, which is defined by its radius. It is assumed that the draught is half the radius and that the maximum stroke equals the draught. The radius range chosen is 1–5 m, on an equally spaced grid with an interval of 0.25 m. For each radius value, the annual average power, using CC, PS, and the WbW method WG/A, is evaluated. To do this, the average power for each of the total 99 sea states in Fig. 8 (right) is computed, for eight realizations of each sea state, and the results are further averaged to get annual values. The design objective function is defined as the annual average power per characteristic length (the cube root of the submerged volume) [42]. The results are shown in Fig. 12.

It is easy to see the difference between the use of an unconstrained optimal controller (CC) and a constrained optimal controller (PS/MPC) in this co-design exercise. The CC result suggests that the body size should be as small as possible, since it assumes that the body position is unconstrained, with consequent unrealistic oscillation amplitudes. In other words, a device co-designed with a CC controller may not achieve the performance promised by the co-design process and, in turn, the device size is non-optimal, since it fails to consider the constraints. In contrast, by taking the maximum stroke into account, PS and MPC give an optimal size range that is between 2–3 m, which corresponds to the actual achievable performance. It is also worth noting that, in Fig. 12, the CC and PS/MPC curves converge as the size increases, since the required oscillation for a large device is small, so the constraints are inactive. Finally, the proposed WbW evaluator gives an optimal size range very close to PS/MPC, successfully fulfilling the goal of accurate and fast control co-design. To compute the performance curves in Fig. 12, the PS-based co-design calculation consumes more than 13 h, while the WbW method uses less than five minutes, which is a significant computational superiority. Note that if constraints other than the maximum displacement are to be considered, the numerical WbW evaluator needs to be used, with a much less, but still significant, computation acceleration than PS.

It should be noted that this study focuses on the control evaluator, rather than the design optimizer. The above results are based on a one-dimensional design case using parameter sweep, to illustrate the

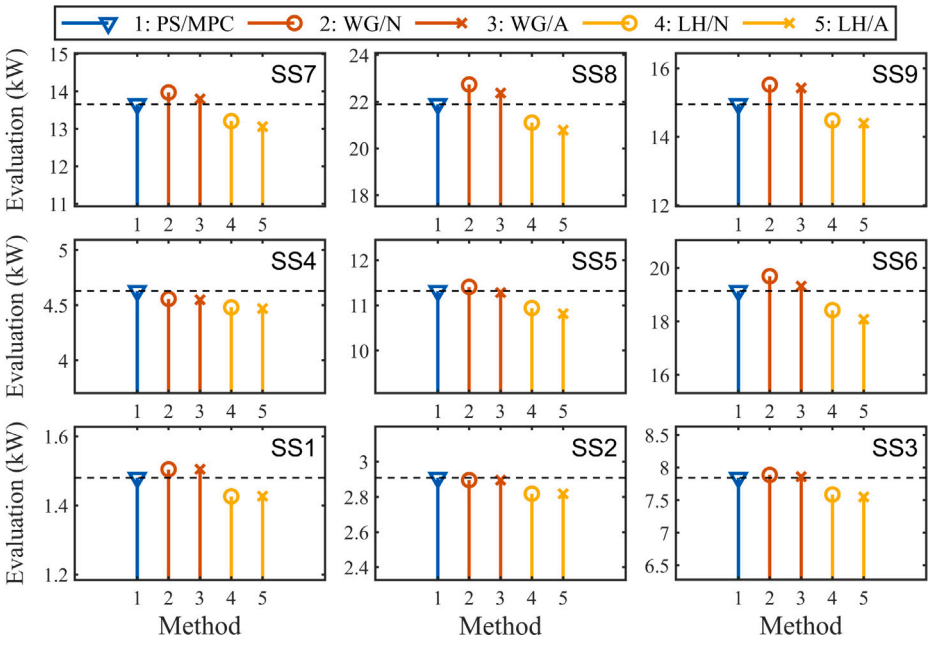

Fig. 9. Average power, for the nine sea states documented in Fig. 8, estimated by PS/MPC, WG/N, WG/A, LH/N, and LH/A. Note that MPC and PS give identical results, so only the PS results are presented and denoted as 'PS/MPC'.

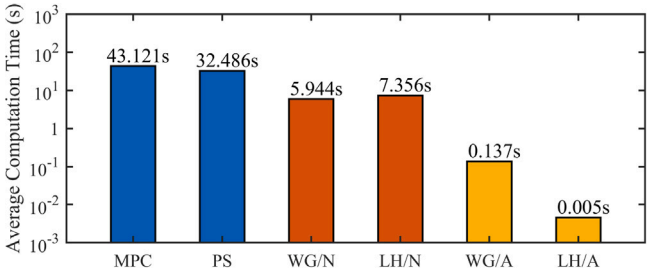

Fig. 10. Average computation times of MPC, PS, WG/A, LH/A, WG/N, and LH/N, with each of MPC, PS, WG/A and WG/N evaluated for eight sea-state realizations.

evaluation efficacy. The WbW method, however, can be combined with, e.g., derivative-based optimizers, to address high-dimensional design problems, which is for future work.

6. Conclusion

The optimal constrained control performance of WECs can be evaluated in a simple way. On the one hand, by adopting the approximations of local radiation damping and wave-by-wave independence, an analytical (A) optimal control solution can be derived for each half wave of the WEF under maximum stroke limitation. On the other hand, the joint distribution of half-wave amplitude and duration can be obtained using either wave signal generation (WG) or the LH model (LH). The combination of the half-wave control solution and half-wave parameter distribution forms the WbW method, yielding an easy calculation of the average power. If a maximum PTO force is also specified, the WbW method can be generalized by incorporating a PS control calculation to obtain a numerical (N) solution. In summary, four WbW evaluator variations can be obtained: WG/A, LH/A, WG/N, and LH/N.

The assumptions taken in the WbW method are verified to be effective for performance evaluation. Using a local radiation damping parameter instead of the exact radiation convolution kernel yields only a limited error, as does using a wave-by-wave-separated calculation, rather than employing a long-term wave calculation. However, in obtaining the half-wave distribution, the LH model exhibits a certain deviation compared with the exact data distribution, and consequently, it causes the main error in the final average power estimation. So, it is recommended to use WG/A for maximum stroke only, and WG/N for general constraints. The WbW evaluator yields accurate and fast evaluation results on multiple bodies, across multiple sea states, and multiple constraints. Compared with PS, the overall evaluation error of the WbW method can be kept below 5%, while the computational speed is orders of magnitude faster under the stroke constraint (where WG/A is utilized) and several times faster when a PTO force constraint is further involved (where WG/N is utilized), so the WbW methods can now be accurately located on the controller continuum in Fig. 2 to get Fig. 13. In addition, the WbW method can avoid the difficulty of control tuning in MPC and PS, as described in Appendix. In co-design of WECs, it is crucial to use an optimal constrained controller. An unconstrained controller such as CC will yield an unrealistic design result. By contrast, the WbW evaluator gives almost the same design result as PS, one of the ideal optimal constrained control options, but the computation time is reduced from over 13 h to less than five minutes.

Some limitations of this study are worth noting. First, the focus is on a heaving point-absorber WEC, frequently used in WEC control research, and possible uses of the WbW technique in other WEC types is a direction for future work. Second, the results are limited to the considered system model (linear Cummins' equation) and constraints (displacement and PTO force). However, the generalized WbW method can naturally be applied to address, e.g., nonlinear models and constraints such as the maximum PTO power. Third, from its working principle, the WbW method is currently limited to single-body cases, and handling WEC array problems would require further, fundamental, extensions of the technique. Moreover, the computational performance of both MPC and PS relies heavily on control parameter tuning, and the current results are based on a specific control tuning strategy. However, given the extent of tuning consideration, it is deemed a fair comparison for the WbW strategy. Finally, the co-design case study provided in the paper is a one-dimensional parameter sweep. Advanced outer-loop optimizers were not explored with the control evaluator. Note that a numerically sensitive control evaluator could cause certain undesirable outcomes in co-design optimization.

In addition, in addition to control evaluation, co-design also involves computational complexities in the calculation of hydrodynamics. Surrogate models are an additional tool to tackle, uniformly, the computational challenge of WEC co-design.

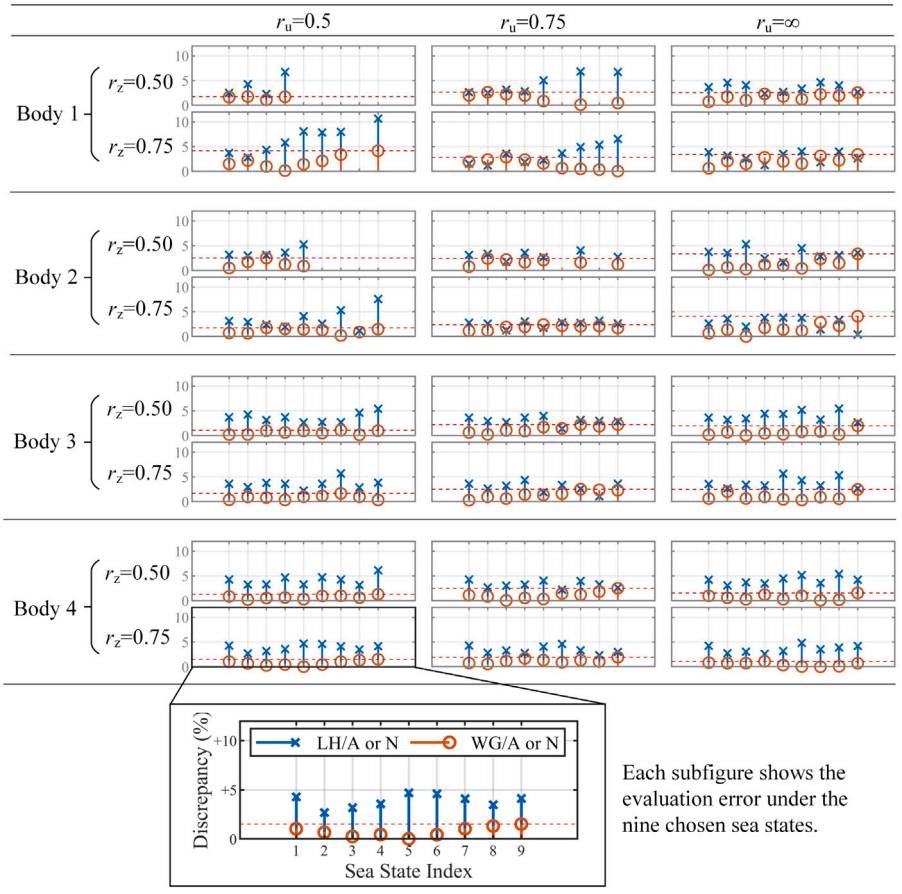

Fig. 11. Comprehensive fidelity testing results (discrepancy in absolute value). When the PTO force is unconstrained, the results are obtained using WG/A and LH/A, otherwise WG/N and LH/N are employed. The missing bars mean no feasible control solution exists.

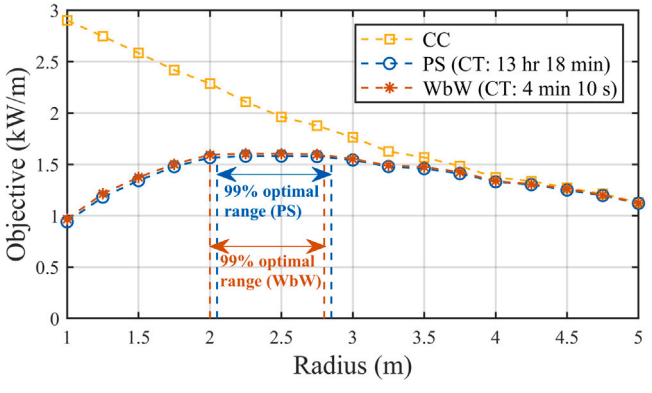

Fig. 12. Co-design results: the optimal device size range in terms of annual average power per characteristic length. CT: computation time.

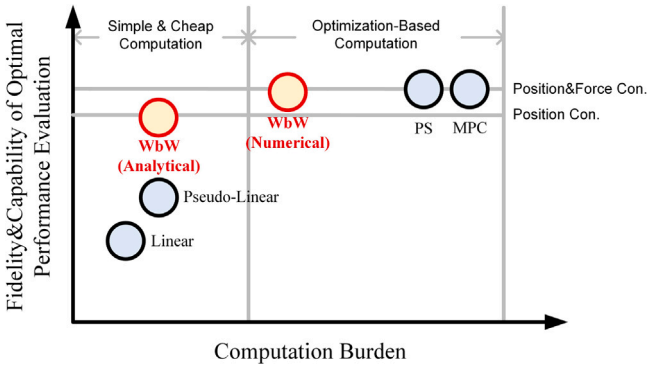

Fig. 13. The fidelity&capability-computation relationship of the controller continuum including the WbW methods (for indicative use, not to scale). Con.: constrained.

CRediT authorship contribution statement

Zechuan Lin: Writing – original draft, Visualization, Validation, Software, Methodology, Investigation, Conceptualization. **Xuanrui Huang:** Validation, Investigation, Formal analysis, Data curation. **Xi Xiao:** Supervision, Resources, Project administration, Funding acquisition, Formal analysis. **John V. Ringwood:** Writing – original draft, Visualization, Supervision.

Declaration of competing interest

The authors declare the following financial interests/personal relationships which may be considered as potential competing interests: Xi Xiao reports financial support was provided by National Natural Science Foundation of China. Xi Xiao reports financial support was provided by National Key Research and Development Program of China. If there are other authors, they declare that they have no known competing financial interests or personal relationships that could have appeared to influence the work reported in this paper.

Acknowledgements

This work is supported by the National Natural Science Foundation of China (Grant No. 52337002, U1806224, and 51977008) and the National Key Research and Development Program of China (Grant No. 2020YFE0205400).

Appendix. Tuning of the benchmark MPC and PS control

The control tuning strategy for both MPC and PS, for co-design, is a challenging task, due to the following factors: (1) there exist multiple control parameters for both controllers, (2) there are a wide range of WEC scenarios (i.e., body geometries, sea states, and constraint settings) to be examined in co-design, and (3) the relationship between control parameters and control evaluation accuracy is *different* in different WEC scenarios. The control parameters should be optimized to maintain the accuracy under all WEC scenarios with the smallest computational burden. To this end, ideally, one needs to first conduct a sensitivity analysis for the control parameters. However, it would be meaningless to conduct the sensitivity analysis for all possible combination of WEC geometries, sea states, and constraints, since the corresponding computational burden is much heavier than the co-design exercise itself. Here, a simplified tuning strategy is proposed, for both MPC and PS, based on some 'extreme' scenarios involved in this study:

- For the body size, only the smallest body with a radius of 1 m (Body A1) and the largest body with a radius of 5 m (Body A2) are considered. The body draught is assumed to be half the radius.
- For the sea state, only the mildest sea state with $H_s = 0.6$ m and $T_p = 4$ s (SS A1) and the most energetic sea state with $H_s = 1.4$ m and $T_p = 7$ s (SS A2) are considered.
- For the constraints, only the tightest constraint with Z_m set to half of the body draught (Con. A1), and the loosest constraint with Z_m set to the body draught (Con. A2), are considered. The PTO force is assumed unconstrained.

Hence, there are eight possible combinations of body size, sea state, and constraint settings. A sensitivity analysis of the control parameters for each scenario will be conducted, and it is expected that the result can be somewhat 'representative' for other scenarios as well.

As the basic setting, each run of control evaluation corresponds to a 100-second operation, and the wave excitation force signal is generated using a Fourier series with a fundamental frequency of $f_0 = \omega_0/(2\pi) = 0.01$ Hz (with a period of 100 s). The Fourier series is truncated at the frequency where the wave excitation force spectral density is less than 0.5% of the maximum value.

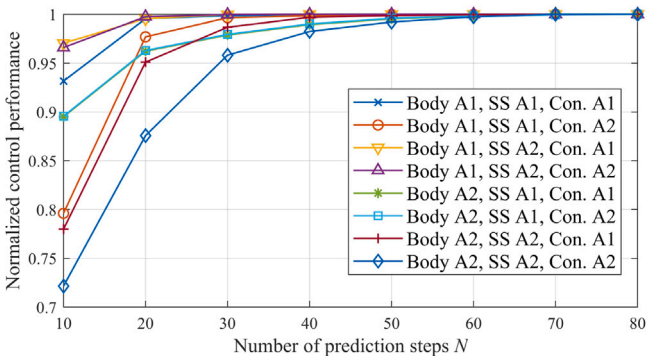

Fig. A.14. Relationship between MPC performance and N in eight extreme scenarios.

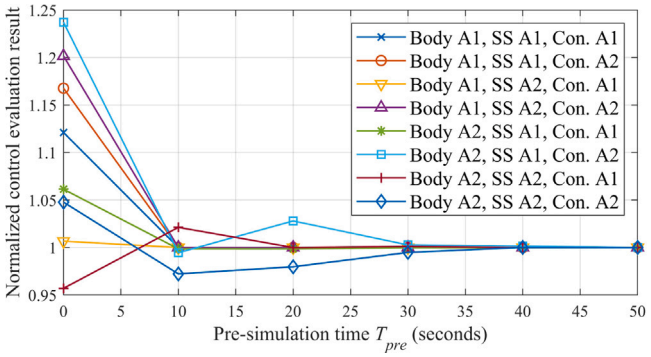

Fig. A.15. Relationship between MPC evaluation and T_{pre} in eight extreme scenarios.

A.1. MPC tuning

MPC, for co-design, has two main parameters to tune, which are the sampling period T_s and the number of prediction steps N (so the prediction time horizon is NT_s). As a good standard for simulation, the sampling period is set according to the cut-off frequency f_c of the system (which is defined as the frequency at which the force-to-velocity response amplitude decreases to $1/\sqrt{2}$ of its maximum value), in order to maintain discretization accuracy. In this study, T_s is chosen to satisfy $T_s < 1/(20f_c)$ and, within this upper bound, T_s is set to be the maximum value within the set {0.1,0.125,0.16,0.2} s, in order to keep the total number of simulation steps as an integer. Then, the relationships between N and MPC performance, under the eight scenarios considered, are shown in Fig. A.14. Accordingly, since the MPC computational burden increases with N, $N = 60$ is selected throughout the co-design study to give accurate evaluation without involving excessive computation.

In addition, since co-design requires a representative power assessment, the steady-state performance of MPC should be assessed, and any effects of the initial state should be eliminated. Hence, the simulation should be started before the 100-second evaluation horizon, with a time interval for the system to reach steady state. This interval is denoted as T_{pre}. The MPC evaluation result, with different T_{pre} values, is shown in Fig. A.15. It can be seen that a small T_{pre} can lead to significant deviation from the accurate evaluation. Hence, T_{pre} is selected to be 40 s throughout the study; the total simulation time for MPC is therefore 140 s.

A.2. PS control tuning

PS control has two main parameters to tune, which are the number of frequency components $N_f = m/2$ (with a fundamental frequency of $f_0 = 0.01$ Hz, the same as the wave spectrum) and the number

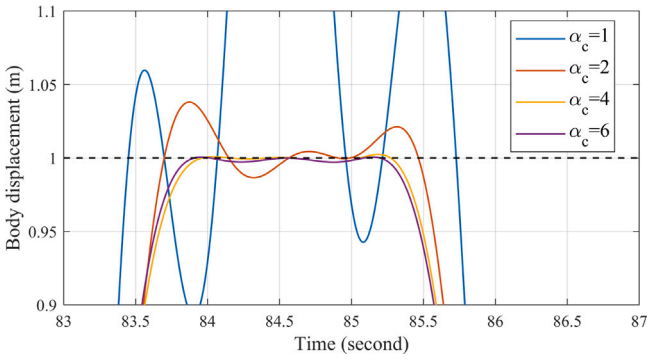

Fig. A.16. Body displacement profile solved by PS under different α_c.

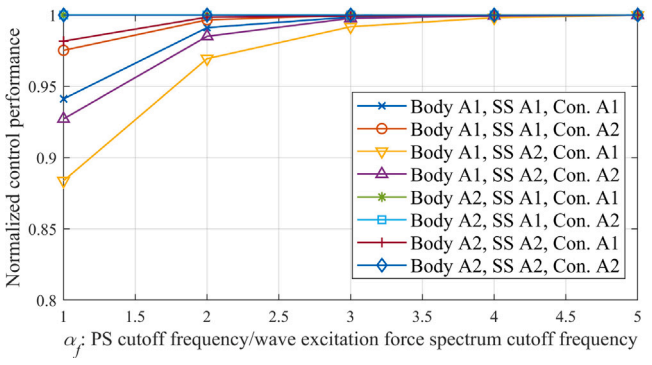

Fig. A.17. Relationship between PS performance and α_f in eight extreme scenarios.

Table A.2
Evaluation results and computation time of receding-horizon MPC and global MPC (body radius 2 m, H_s = 1 m, T_p = 6 s, Z_m = 1 m).

Receding-horizon MPC		Global MPC	
Evaluation	Computation time	Evaluation	Computation time
10.53 kW	6.11 s	10.53 kW	11.60 s

of collocation points (N_c + 1) to apply the constraints, which should be uniformly distributed over the 100-second time range (with an interval of $1/(N_c f_0)$ s). In principle, N_c should be set small to reduce the computational burden (number of constraints in PS optimization); meanwhile, N_c should provide a sufficiently dense time grid, according to the highest frequency component of system response, which is $N_f f_0$, to avoid significant violation of the constraints. The 'collocation point ratio' α_c is defined as the ratio between the period of the highest-frequency component, which is $1/(N_f f_0)$, to the interval of collocation points, which is $1/(N_c f_0)$, and there is $N_c = \alpha_c N_f$; a larger α_c means a denser collocation point distribution. For the optimized N_f (to be discussed later), the effect of α_c on the control trajectory is shown in Fig. A.16, and similar observations can be made for other WEC scenarios. Accordingly, α_c = 4 is selected throughout this study, with the remaining control variable being N_f.

One of the PS control features is that high-frequency components outside the wave excitation force spectrum are involved. Hence, let N_f be dependent on the wave excitation force spectrum cut-off frequency $N_{wc} = n_2\omega_0$, and define $N_f = \alpha_f N_{wc}$. The relationship between α_f and PS control performance, under the considered eight scenarios, is shown in Fig. A.17. It can be seen that, similar to the MPC case, since a larger α_f results in a heavier computational burden, α_f = 3 is selected throughout this study, to strike a balance between accuracy and computation.

A.3. Global MPC for control evaluation

Additionally, as mentioned in Section 3.2, another alternative to receding-horizon MPC is global MPC. Based on the T_s, N, and T_{pre} selected in Appendix A.1, global MPC directly solves the control problem over the entire operating horizon, which is (T_{pre} + 100 + NT_s) s. An illustrative comparison between the two MPC approaches, in a specific WEC scenario, is presented in Table A.2. It can be seen that the evaluation results are the same, while global MPC suffers from a much longer computation time, due to its high optimization dimension. Similar results can be obtained in other scenarios. Hence, receding-horizon MPC (referred to as 'MPC') has been used in this study.

References

[1] J.V. Ringwood, S. Zhan, N. Faedo, Empowering wave energy with control technology: Possibilities and pitfalls, Annu. Rev. Control 55 (2023) 18–44.
[2] X. Xiao, X. Huang, Q. Kang, A hill-climbing-method-based maximum-power-point-tracking strategy for direct-drive wave energy converters, IEEE Trans. Ind. Electron. 63 (1) (2015) 257–267.
[3] W. Sheng, R. Alcorn, A. Lewis, On improving wave energy conversion, part I: Optimal and control technologies, Renew. Energy 75 (2015) 922–934.
[4] N. Faedo, S. Olaya, J.V. Ringwood, Optimal control, MPC and MPC-like algorithms for wave energy systems: An overview, IFAC J. Syst. Control 1 (2017) 37–56.
[5] P.B. Garcia-Rosa, J.V. Ringwood, On the sensitivity of optimal wave energy device geometry to the energy maximizing control system, IEEE Trans. Sustain. Energy 7 (1) (2015) 419–426.
[6] L.Y. Pao, D.S. Zalkind, D.T. Griffith, M. Chetan, M.S. Selig, G.K. Ananda, C.J. Bay, T. Stehly, E. Loth, Control co-design of 13 MW downwind two-bladed rotors to achieve 25% reduction in levelized cost of wind energy, Annu. Rev. Control 51 (2021) 331–343.
[7] J. Hals, J. Falnes, T. Moan, Constrained optimal control of a heaving buoy wave-energy converter, J. Offshore Mech. Arct. Eng. 133 (1) (2011) 011401.
[8] Z. Lin, X. Huang, X. Xiao, Fast model predictive control system for wave energy converters with wave tank tests, IEEE Trans. Ind. Electron. 70 (7) (2022) 6887–6897.
[9] A. Mérigaud, J.V. Ringwood, Free-surface time-series generation for wave energy applications, IEEE J. Ocean. Eng. 43 (1) (2017) 19–35.
[10] G. Bacelli, J.V. Ringwood, Numerical optimal control of wave energy converters, IEEE Trans. Sustain. Energy 6 (2) (2014) 294–302.
[11] C.A.M. Ströfer, D.T. Gaebele, R.G. Coe, G. Bacelli, Control co-design of power take-off systems for wave energy converters using WecOptTool, IEEE Trans. Sustain. Energy 14 (2023) 2157–2167.
[12] H. Abdulkadir, O. Abdelkhalik, Optimization of heterogeneous arrays of wave energy converters, Ocean Eng. 272 (2023) 113818.
[13] A.H. Izadparast, J.M. Niedzwecki, Estimating the potential of ocean wave power resources, Ocean Eng. 38 (1) (2011) 177–185.
[14] W. Cummins, et al., The Impulse Response Function and Ship Motions, Tech. Rep., Department of the Navy, David Taylor Model Basin Bethesda, MD, USA, 1962.
[15] D. García-Violini, Y. Peña-Sanchez, N. Faedo, J.V. Ringwood, An energy-maximising linear time invariant controller (LiTe-Con) for wave energy devices, IEEE Trans. Sustain. Energy 11 (4) (2020) 2713–2721.
[16] M. Shadman, S.F. Estefen, C.A. Rodriguez, I.C. Nogueira, A geometrical optimization method applied to a heaving point absorber wave energy converter, Renew. Energy 115 (2018) 533–546.
[17] V. Piscopo, G. Benassai, L. Cozzolino, R. Della Morte, A. Scamardella, A new optimization procedure of heaving point absorber hydrodynamic performances, Ocean Eng. 116 (2016) 242–259.
[18] A. McCabe, Constrained optimization of the shape of a wave energy collector by genetic algorithm, Renew. Energy 51 (2013) 274–284.
[19] A. Garcia-Teruel, O. Roberts, D.R. Noble, J.C. Henderson, H. Jeffrey, Design limits for wave energy converters based on the relationship of power and volume obtained through multi-objective optimisation, Renew. Energy 200 (2022) 492–504.
[20] H. Abdulkadir, A. Ellithy, A. Ossama, Heterogeneous WEC array optimization using the hidden genes genetic algorithm, in: Proceedings of the European Wave and Tidal Energy Conference, Vol. 15, Bilbao, Spain, 2023.
[21] A.C. O'Sullivan, G. Lightbody, Co-design of a wave energy converter using constrained predictive control, Renew. Energy 102 (2017) 142–156.

[22] G. Li, M.R. Belmont, Model predictive control of sea wave energy converters—Part I: A convex approach for the case of a single device, Renew. Energy 69 (2014) 453–463.
[23] G. Bacelli, J.V. Ringwood, A geometric tool for the analysis of position and force constraints in wave energy converters, Ocean Eng. 65 (2013) 10–18.
[24] M. Blanco, M. Lafoz, D. Ramirez, G. Navarro, J. Torres, L. Garcia-Tabares, Dimensioning of point absorbers for wave energy conversion by means of differential evolutionary algorithms, IEEE Trans. Sustain. Energy 10 (3) (2018) 1076–1085.
[25] Y. Peña-Sanchez, D. García-Violini, J.V. Ringwood, Control co-design of power take-off parameters for wave energy systems, IFAC-PapersOnLine 55 (27) (2022) 311–316.
[26] L. Wang, J.V. Ringwood, Control-informed ballast and geometric optimisation of a three-body hinge-barge wave energy converter using two-layer optimisation, Renew. Energy 171 (2021) 1159–1170.
[27] Y. Peña-Sanchez, D. García-Violini, M. Penalba, A. Zarketa-Astigarraga, F. Ferri, V. Nava, J.V. Ringwood, Control co-design for wave energy farms: Optimisation of array layout and mooring configuration in a realistic wave climate, Renew. Energy 227 (2024) 120506.
[28] M.C. Devin, D.T. Gaebele, C.A.M. Ströfer, J.T. Grasberger, J. Lee, R.G. Coe, G. Bacelli, High-dimensional control co-design of a wave energy converter with a novel pitch resonator power takeoff system, Ocean Eng. 312 (2024) 119124.
[29] N. Faedo, G. Scarciotti, A. Astolfi, J.V. Ringwood, Nonlinear energy-maximizing optimal control of wave energy systems: A moment-based approach, IEEE Trans. Control Syst. Technol. 29 (6) (2021) 2533–2547.
[30] C. Auger, A. Mérigaud, J.V. Ringwood, Receding-horizon pseudo-spectral control of wave energy converters using periodic basis functions, IEEE Trans. Sustain. Energy 10 (4) (2018) 1644–1652.
[31] A. Mérigaud, J.V. Ringwood, Towards realistic non-linear receding-horizon spectral control of wave energy converters, Control Eng. Pract. 81 (2018) 145–161.
[32] R. Genest, J.V. Ringwood, Receding horizon pseudospectral control for energy maximization with application to wave energy devices, IEEE Trans. Control Syst. Technol. 25 (1) (2016) 29–38.
[33] A. Babarit, G. Delhommeau, Theoretical and numerical aspects of the open source BEM solver NEMOH, in: Proceedings of the European Wave and Tidal Energy Conference, Vol. 11, Nantes, France, 2015.
[34] F. Fusco, J.V. Ringwood, A simple and effective real-time controller for wave energy converters, IEEE Trans. Sustain. Energy 4 (1) (2012) 21–30.
[35] J. Falnes, A. Kurniawan, Ocean Waves and Oscillating Systems: Linear Interactions Including Wave-Energy Extraction, vol. 8, Cambridge University Press, 2020.
[36] M.S. Longuet-Higgins, On the joint distribution of wave periods and amplitudes in a random wave field, Proc. R. Soc. A 389 (1797) (1983) 241–258.
[37] R. Sobey, The distribution of zero-crossing wave heights and periods in a stationary sea state, Ocean Eng. 19 (2) (1992) 101–118.
[38] P.A. Brodtkorb, P. Johannesson, G. Lindgren, I. Rychlik, J. Rydén, E. Sjö, WAFO—A matlab toolbox for analysis of random waves and loads, in: 10th Inernational Offshore and Polar Engineering Conference, OnePetro, Seattle, USA, 2000.
[39] G. Lindgren, Gaussian integrals and rice series in crossing distributions—To compute the distribution of maxima and other features of Gaussian processes, Statist. Sci. 34 (1) (2019) 100–128.
[40] National marine data center, national science and technology resource sharing service platform of China, 2023, http://mds.nmdis.org.cn/. (Accessed: 10 April 2023).
[41] J. Goggins, W. Finnegan, Shape optimisation of floating wave energy converters for a specified wave energy spectrum, Renew. Energy 71 (2014) 208–220.
[42] B. Guo, J.V. Ringwood, Geometric optimisation of wave energy conversion devices: A survey, Appl. Energy 297 (2021) 117100.